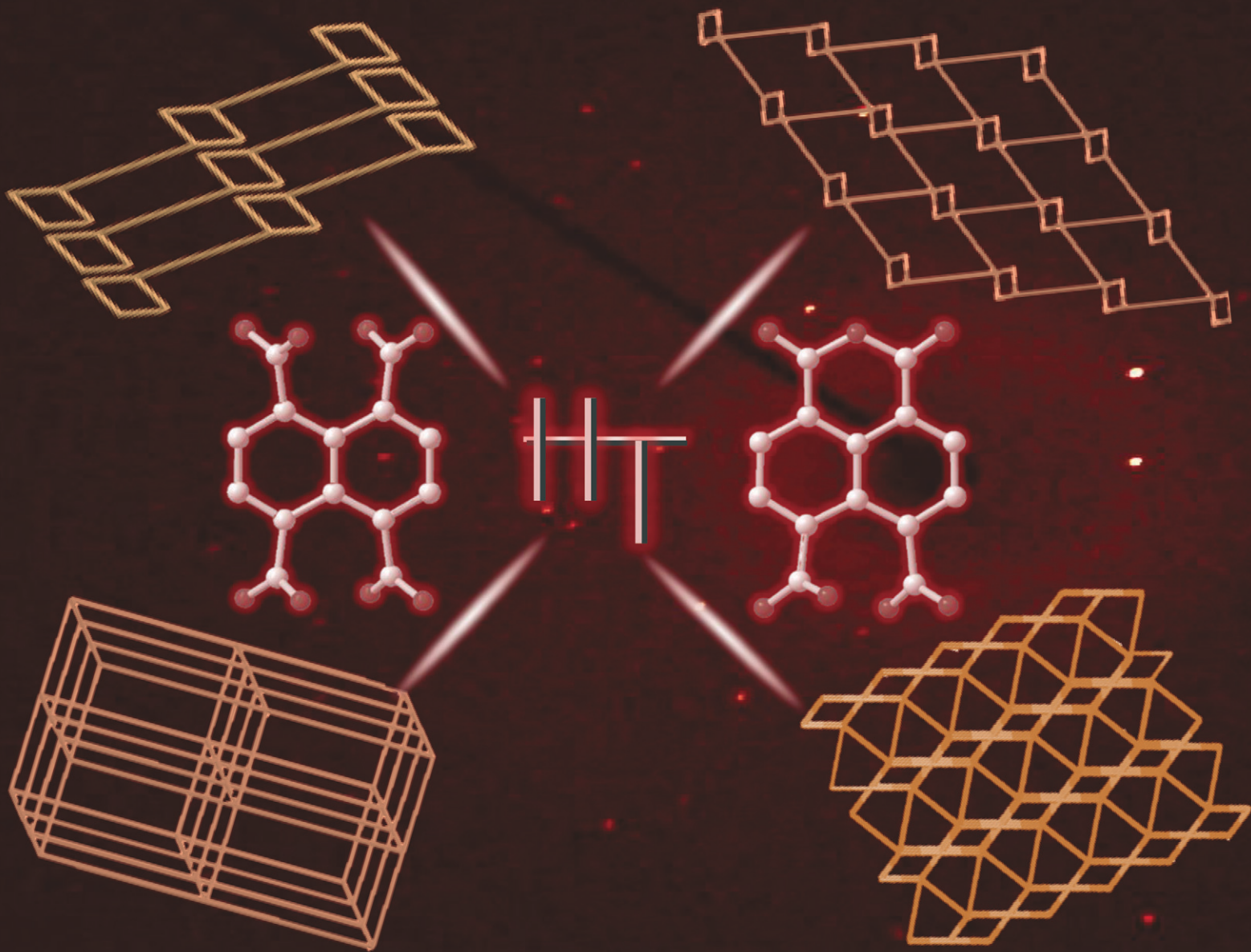


CrystEngComm

rsc.li/crystengcomm




ISSN 1466-8033

PAPER

Shih-Miao Liu, Jhy-Der Chen *et al.*
Coordination polymers constructed from
bis-pyridyl-bis-amides and 1,4,5,8-naphthalenetetracarboxylic
acid: ligand transformation and metal ion sensing


Cite this: *CrystEngComm*, 2025, 27, 606

Coordination polymers constructed from bis-pyridyl-bis-amides and 1,4,5,8-naphthalenetetracarboxylic acid: ligand transformation and metal ion sensing†

Wei-Hao Chen,^a Yen-Hsin Chen,^a Kedar Bahadur Thapa,^b Shih-Miao Liu^{*c} and Jhy-Der Chen  ^{*a}

Hydrothermal reactions of 1,4,5,8-naphthalenetetracarboxylic acid (1,4,5,8-H₄NTC) with various bis-pyridyl-bis-amides, *N,N'*-di(pyridin-3-yl)adipamide (L¹), *N,N'*-di(pyridin-3-yl)succinamide (L²), *N,N'*-di(pyridin-3-yl)oxalamide (L³) or *N,N'*-bis(pyridin-3-ylmethyl)oxalamide (L⁴) and transition metal salt afforded seven coordination polymers (CPs) and one dinuclear complex, including [Cd(L¹)_{0.5}(1,4,5,8-NTC')(H₂O)₂]_n (1,4,5,8-H₂NTC' = 1,4,5,8-naphthalenetetracarboxylic acid 1,8-monoanhydride), **1**, {[Zn(L²)_{0.5}(1,4,5,8-NTC')(H₂O)₂·H₂O]_n, **2**, {[Cd(L²)_{0.5}(1,4,5,8-NTC')(H₂O)₂·H₂O]_n, **3**, {[Zn(L⁵)(1,4,5,8-NTC')(H₂O)]·0.5OA]_n, {L⁵ = 2,7-di(pyridin-3-yl)benzo[*lmn*][3,8]phenanthroline-1,3,6,8(2*H*,7*H*)-tetraone}, **4**, [Cd(L⁵)(1,4,5,8-NTC')(H₂O)]_n, **5a**, {[Cd(L⁵)(1,4,5,8-NTC')(H₂O)]·2H₂O]_n, **5b**, [Zn₂(L⁴)(1,4,5,8-NTC')₂(H₂O)₆], **6**, and {[Cd(L⁴)(1,4,5,8-NTC')_{0.5}(H₂O)]·0.5H₂O]_n (1,4,5,8-H₄NTC = 1,4,5,8-naphthalenetetracarboxylic acid), **7**. These CPs and the dinuclear complex were structurally characterized by using X-ray single-crystal diffraction. CPs **1**, **2**, and **3** exhibit one-dimensional (1D) structures with the 2,3C2 topology and **4** and **5** display two-dimensional (2D) structures with the 2,4L1 topology, whereas **6** is a dinuclear complex and **7** shows a three-dimensional (3D) framework with the **mog** topology. Ligand transformations from 1,4,5,8-H₄NTC to 1,4,5,8-NTC'²⁻ and L³ to L⁵ are observed. The evaluation of the metal ion sensing properties of **1**, **2**, **3**, **6**, and **7** shows that **7** has the highest potential for detecting Fe³⁺ ions in aqueous solution with 1.06 × 10³ M⁻¹ and 1.99 × 10⁻⁴ M for the Stern–Volmer constant (*K*_{SV}) and the limit of detection (LOD), respectively.

Received 4th November 2024,
Accepted 19th December 2024

DOI: 10.1039/d4ce01119h

rsc.li/crystengcomm

Introduction

Coordination polymers (CPs) have been widely researched by scientists in recent years due to their intriguing structural diversity and various applicable functions.^{1,2} By careful evaluation of the factors that govern the structural diversity of CPs, including metal types, the softness, length, coordination ability and coordination direction of organic ligands, and reaction conditions such as solvent, temperature and reaction

time, CPs with different characteristics can be designed.^{3,4} Through metal–ligand bonds, CPs form infinitely extending one- (1D), two- (2D) or three-dimensional (3D) structures.^{5–8} CPs are applicable in various fields such as gas storage and separation, sensors, magnetism, conductive material, catalysis, degradation of dyes or pollutants, drug delivery, *etc.*^{9–19}

Di-, tri- and tetracarboxylate ligands have been used frequently to prepare CPs with interesting structural topologies. The bis-pyridyl-bis-amide (bpba)-based CPs constructed from 1,2,4,5-benzenetetracarboxylic acid (1,2,4,5-H₄BETC) have been extensively investigated.^{8,20–22} Structural comparisons of the Co(II),^{20,21} Zn(II)²² and Cu(II)⁸ CPs thus prepared indicate that their structural diversity is manipulated by the flexibility of the bpba ligands, which is also subject to the coordination and co-crystallization of the solvent molecules. The structural diversity of these CPs demonstrates that the combination of the flexible bpba and 1,2,4,5-H₄BETC under suitable conditions may form diverse and interesting structures.

To further investigate the role of the tetracarboxylate ligand in determining the structural diversity of bpba-based CPs,

^a Department of Chemistry, Chung Yuan Christian University, Chung-Li, Taiwan, R. O.C.. E-mail: jdchen@cycu.edu.tw

^b Makawanpur Multiple Campus, affiliated to Tribhuvan University, Municipality Rd, Hetauda, Nepal

^c Center for General Education, Hsin Sheng Junior College of Medical Care and Management, Longtan, Taiwan, R.O.C.. E-mail: lsm0301@hsc.edu.tw

† Electronic supplementary information (ESI) available: PXRD patterns (Fig. S1–S8, S17–S21 and S32). TGA curves (Fig. S9–S16). Emission spectra (Fig. S22–S31 and S38). UV-vis absorption spectrum (Fig. S33). EDX data (Fig. S34). IR spectra (Fig. S35). XPS spectra (Fig. S36 and S37). Nitrogen adsorption–desorption isotherm (Fig. S39–S48). CCDC no. 2395512–2395519 contain the supplementary crystallographic data for this paper. For ESI and crystallographic data in CIF or other electronic format see DOI: <https://doi.org/10.1039/d4ce01119h>


1,4,5,8-naphthalenetetracarboxylic acid (1,4,5,8-H₄NTC) was invoked to react with the bpba ligand, *N,N'*-di(pyridin-3-yl) adipamide (**L**¹), *N,N'*-di(pyridin-3-yl)succinamide (**L**²), *N,N'*-di(pyridin-3-yl)oxalamide (**L**³) or *N,N'*-bis(pyridin-3-ylmethyl) oxalamide (**L**⁴), and Zn(II) or Cd(II) salt to synthesize new CPs. Fig. 1 shows the structures of the bpba ligands and 1,4,5,8-H₄NTC used in this investigation. Herein, the syntheses and structures of [Cd(**L**¹)_{0.5}(1,4,5,8-NTC')(H₂O)₂]_n (1,4,5,8-H₂NTC' = 1,4,5,8-naphthalenetetracarboxylic acid 1,8-monoanhydride), **1**, {[Zn(**L**²)_{0.5}(1,4,5,8-NTC')(H₂O)₂·H₂O]_n, **2**, {[Cd(**L**²)_{0.5}(1,4,5,8-NTC')(H₂O)₂·H₂O]_n, **3**, {[Zn(**L**⁵)(1,4,5,8-NTC')(H₂O)]·0.5OA]_n, (**L**⁵ = 2,7-di(pyridin-3-yl)benzo[*lmn*][3,8]phenanthroline-1,3,6,8(2*H*,7*H*)-tetraone), **4**, [Cd(**L**⁵)(1,4,5,8-NTC')(H₂O)]_n, **5a**, {[Cd(**L**⁵)(1,4,5,8-NTC')(H₂O)]·2H₂O]_n, **5b**, [Zn(**L**⁴)(1,4,5,8-NTC')₂(H₂O)₆], **6**, and {[Cd(**L**⁴)(1,4,5,8-NTC')_{0.5}(H₂O)]·0.5H₂O]_n, **7**, form the subject of this report. The structural diversity and ligand transformation of these CPs and the complex are discussed and their metal ion sensing capabilities evaluated.

Experimental details

General procedures

IR spectra (KBr disk) were obtained with a Thermo Nicolet IS5 FT-IR spectrometer. Elemental analyses were performed on an Elementar Vario EL III or an Elementar Vario EL cube type analyzer. Thermal gravimetric analyses (TGA) measurements were carried out on a SII Nano Technology Inc. TG/DTA 6200 over the temperature range of 30 to 900 °C at a heating rate of 10 °C min⁻¹ under N₂. Powder X-ray diffraction measurements were performed on a Bruker D2 PHASER diffractometer with CuK_α (λ_α = 1.54 Å) radiation. X-ray photoelectron spectroscopy (XPS) was on performed on a ULVAC-PHI (Quantex) spectrometer. Emission spectra were collected by using a Hitachi F-7000 spectrometer and the setting of PMT voltage was 250 V. Gas sorption measurements were conducted on a Micromeritics ASAP 2020 system.

Materials

The reagent Cd(OAc)₂·2H₂O and Zn(OAc)₂·2H₂O was purchased from Fisher Scientific Co. and 1,4,5,8-

naphthalenetetracarboxylic acid was purchased from Nova Materials Co., Ltd. The ligands **L**¹, **L**², **L**³, **L**⁴, and **L**⁵ was prepared according to published procedures.^{12,23}

Preparation of [Cd(L**¹)_{0.5}(1,4,5,8-NTC')(H₂O)₂]_n, **1**.** A mixture of Cd(OAc)₂·2H₂O (0.053 g, 0.20 mmol), **L**¹ (0.030 g, 0.10 mmol) and 1,4,5,8-H₄NTC (0.030 g, 0.10 mmol) in 10 mL of H₂O was sealed in a 23 mL Teflon-lined stainless steel autoclave, which was heated under autogenous pressure to 120 °C for two days and then the reaction system was cooled down to room temperature over 48 hours. The colorless crystals suitable for single-crystal X-ray diffraction were obtained. Yield: 0.030 g (26%). Anal. calcd for C₂₂H₁₇N₂O₁₀Cd (MW = 581.79): C, 45.42; H, 2.95; N, 4.82%. Found: C, 45.88; H, 2.62; N, 5.32%. FT-IR (cm⁻¹): 3554(w), 3297(m), 3062(w), 1772(m), 1721(m), 1658(s), 1582(s), 1511(s), 1427(s), 1345(s), 1222(m), 1024(m), 766(m), 698(m).

Preparation of {[Zn(L**²)_{0.5}(1,4,5,8-NTC')(H₂O)₂·H₂O]_n, **2**.** CP **2** was prepared by following similar procedures for **1**, except that a mixture of Zn(OAc)₂·2H₂O (0.022 g, 0.10 mmol), **L**² (0.027 g, 0.10 mmol) and 1,4,5,8-H₄NTC (0.030 g, 0.10 mmol) in 10 mL of H₂O at 100 °C was used. Colorless crystals were obtained. Yield: 0.017 g (32%). Anal. calcd for C₂₁H₁₇N₂O₁₁Zn·0.5H₂O (MW = 529.76): C, 47.61; H, 3.04; N, 5.29%. Found: C, 47.52; H, 2.84; N, 6.03%. FT-IR (cm⁻¹): 3559(w), 3273(m), 3051(w), 1771(m), 1720(m), 1666(s), 1580(s), 1516(s), 1428(s), 1384(s), 1217(m), 1018(m), 769(m), 706(m).

Preparation of {[Cd(L**²)_{0.5}(1,4,5,8-NTC')(H₂O)₂·H₂O]_n, **3**.** CP **3** was prepared by following similar procedures for **1**, except that a mixture of Cd(OAc)₂·2H₂O (0.053 g, 0.20 mmol), **L**² (0.027 g, 0.10 mmol) and 1,4,5,8-H₄NTC (0.030 g, 0.10 mmol) in 10 mL of H₂O at 80 °C was used. Colorless crystals were obtained. Yield: 0.052 g (44%). Anal. calcd for C₂₁H₁₇N₂O₁₁Cd·0.5H₂O (MW = 576.78): C, 43.73; H, 2.80; N, 4.86%. Found: C, 43.72; H, 2.80; N, 5.32%. FT-IR (cm⁻¹): 3560(w), 3375(w), 2937(w), 1778(m), 1725(m), 1579(s), 1425(s), 1384(s), 1339(s), 1290(m), 1214(m), 1158(m), 1030(m), 771(m).

Preparation of {[Zn(L**⁵)(1,4,5,8-NTC')(H₂O)]·0.5OA]_n, **4**.** CP **4** was prepared by following similar procedures for **1**, except that a mixture of Zn(OAc)₂·2H₂O (0.022 g, 0.10 mmol), **L**³ (0.024 g, 0.10 mmol) and 1,4,5,8-H₄NTC (0.030 g, 0.10 mmol) in 10 mL of H₂O was used. Colorless crystals were obtained. Yield: 0.012 g (15%). Anal. calcd for C₃₉H₁₉N₄O₁₄Zn (MW = 832.98): C, 56.23; H, 2.30; N, 6.73%. Anal. calcd for C₃₉H₁₉N₄O₁₄Zn·0.5EDA (MW = 787.96): C, 57.92; H, 2.30; N, 7.11%. Found: C, 57.46; H, 2.19; N, 8.29%. FT-IR (cm⁻¹): 3538(w), 3382(w), 3114(w), 1771(m), 1721(s), 1668(s), 1629(s), 1587(m), 1479(m), 1436(s), 1379(m), 1334(s), 1237(s), 1190(m), 1037(m), 869(m), 769(m).

Preparation of [Cd(L**⁵)(1,4,5,8-NTC')(H₂O)]_n, **5a**.** CP **5a** was prepared by following similar procedures for **1**, except that a mixture of Cd(OAc)₂·2H₂O (0.053 g, 0.20 mmol), **L**³ (0.024 g, 0.10 mmol) and 1,4,5,8-H₄NTC (0.030 g, 0.10 mmol) in 10 mL of H₂O was used. Colorless crystals were obtained. Yield: 0.012 g (7%). Anal. calcd for C₃₈H₂₀N₄O₁₃Cd (MW = 853.02):

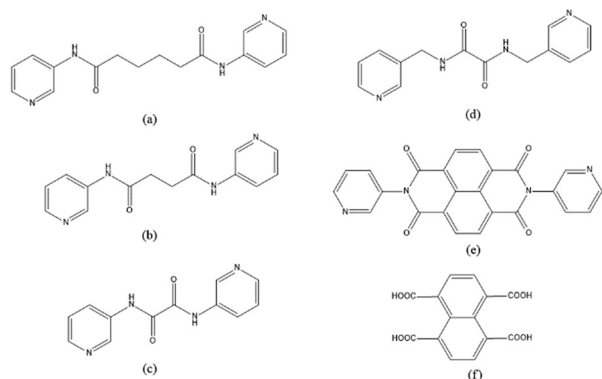


Fig. 1 Structures of (a) **L**¹, (b) **L**², (c) **L**³, (d) **L**⁴, (e) **L**⁵ and (f) 1,4,5,8-H₄NTC.



C, 53.51; H, 2.36; N, 6.57%. Found: C, 54.23; H, 2.01; N, 8.69% FT-IR (cm^{-1}): 3585(m), 3167(w), 2926(w), 1754(m), 1691(s), 1617(s), 1527(s), 1428(m), 1312(s), 1245(w), 1202(w), 1044(w), 872(w), 782(s), 508(s).

Preparation of $\{[\text{Cd}(\text{L}^5)(1,4,5,8\text{-NTC})(\text{H}_2\text{O})]\cdot 2\text{H}_2\text{O}\}_n$, **5b.** CP **5b** was prepared by following similar procedures for **1**, except that a mixture of $\text{Cd}(\text{OAc})_2\cdot 2\text{H}_2\text{O}$ (0.053 g, 0.20 mmol), L^5 (0.021 g, 0.050 mmol) and 1,4,5,8- H_4NTC (0.030 g, 0.10 mmol) in 10 mL of H_2O at 100 °C was used. Colorless crystals were obtained. Yield: 0.020 g (12%). Anal. calcd for $\text{C}_{38}\text{H}_{22}\text{N}_4\text{O}_{14}\text{Cd}$ (MW = 852.98): C, 52.46; H, 2.55; N, 6.43%. Found: C, 52.48; H, 2.53; N, 6.26% FT-IR (cm^{-1}): 3561(m), 3190(w), 3064(m), 1776(m), 1720(s), 1675(s), 1579(s), 1432(s), 1387(s), 1339(s), 1244(m), 1209(m), 1020(s), 765(m).

Preparation of $[\text{Zn}_2(\text{L}^4)(1,4,5,8\text{-NTC})_2(\text{H}_2\text{O})_6]$, **6.** Complex **6** was prepared by following similar procedures for **1**, except that a mixture of $\text{Zn}(\text{OAc})_2\cdot 2\text{H}_2\text{O}$ (0.022 g, 0.10 mmol), L^4 (0.027 g, 0.10 mmol) and 1,4,5,8- H_4NTC (0.030 g, 0.10 mmol) in 10 mL of H_2O at 80 °C was used. Colorless crystals were obtained. Yield: 0.059 g (55%). Anal. calcd for $\text{C}_{42}\text{H}_{34}\text{N}_4\text{O}_{22}\text{Zn}_2$ (MW = 1077.51): C, 46.82; H, 3.18; N, 5.20%. Found: C, 47.82; H, 3.13; N, 4.84%. FT-IR (cm^{-1}): 3552(w), 3292(s), 3062(m), 1773(s), 1719(s), 1665(s), 1592(s), 1509(s), 1429(s), 1385(s), 1330(s), 1277(s), 1217(s), 1019(s), 768(s).

Preparation of $\{[\text{Cd}(\text{L}^4)(1,4,5,8\text{-NTC})_{0.5}(\text{H}_2\text{O})]\cdot \text{H}_2\text{O}\}_n$, **7.** CP **7** was prepared by following similar procedures for **1**, except that a mixture of $\text{Cd}(\text{OAc})_2\cdot 2\text{H}_2\text{O}$ (0.053 g, 0.20 mmol), L^4 (0.027 g, 0.10 mmol) and 1,4,5,8- H_4NTC (0.030 g, 0.10 mmol) in 10 mL of H_2O at 80 °C was used. Colorless crystals were obtained. Yield: 0.044 g (39%). Anal. calcd for $\text{C}_{21}\text{H}_{19}\text{N}_4\text{O}_{7.5}\text{Cd} + 0.25\text{H}_2\text{O}$ (MW = 541.81): C, 45.79; H, 3.29; N, 10.17%. Found: C, 45.59; H, 3.10; N, 10.25%. FT-IR (cm^{-1}): 3561(m), 3201(m), 3064(m), 1772(s), 1721(s), 1585(s), 1546(s), 1528(s), 1385(s), 1328(s), 1158(m), 1019(s), 765(m).

X-ray crystallography

The diffraction data for the CPs and dinuclear complex were collected on a Bruker AXS SMART APEX II CCD diffractometer, which was equipped with a graphite-monochromated $\text{Mo K}\alpha$ ($\lambda_\alpha = 0.71073$ Å) radiation. Data reduction was carried out by standard methods with use of well-established computational procedures.²⁴ The structure factors were obtained after Lorentz and polarization corrections. An empirical absorption correction based on “multi-scan” was applied to the data. The position of some of the heavier atoms were located by the direct or Patterson method. The remaining atoms were found in a series of alternating difference Fourier maps and least-square refinements, while the hydrogen atoms except those of the water molecules were added by using the HADD command in SHELXTL 6.1012.²⁵ The solvent molecules of **5a** were seriously disordered and were squeezed.²⁶ The calculated structure factors of **5a** were thus reported without solvent contribution. Table 1 lists the crystal data for **1–7**.

Results and discussion

Syntheses and ligand transformation

Seven CPs, $[\text{Cd}(\text{L}^1)_{0.5}(1,4,5,8\text{-NTC})(\text{H}_2\text{O})_2]_n$, **1**, $\{[\text{Zn}(\text{L}^2)_{0.5}(1,4,5,8\text{-NTC})(\text{H}_2\text{O})_2]\cdot \text{H}_2\text{O}\}_n$, **2**, $\{[\text{Cd}(\text{L}^2)_{0.5}(1,4,5,8\text{-NTC})(\text{H}_2\text{O})_2]\cdot \text{H}_2\text{O}\}_n$, **3**, $\{[\text{Zn}(\text{L}^5)(1,4,5,8\text{-NTC})(\text{H}_2\text{O})]\cdot 0.5\text{OA}\}_n$, **4**, $[\text{Cd}(\text{L}^5)(1,4,5,8\text{-NTC})(\text{H}_2\text{O})]_n$, **5a**, $\{[\text{Cd}(\text{L}^5)(1,4,5,8\text{-NTC})(\text{H}_2\text{O})]\cdot 2\text{H}_2\text{O}\}_n$, **5b**, and $\{[\text{Cd}(\text{L}^4)(1,4,5,8\text{-NTC})_{0.5}(\text{H}_2\text{O})]\cdot 0.5\text{H}_2\text{O}\}_n$, **7**, and one dinuclear complex, $[\text{Zn}_2(\text{L}^4)(1,4,5,8\text{-NTC})_2(\text{H}_2\text{O})_6]$, **6**, have been synthesized. A distinctive feature showing the transformation from 1,4,5,8- H_4NTC to 1,4,5,8- NTC^{2-} can be observed in **1–6**, presumably due to the condensation of the carboxylate groups of 1,4,5,8- H_4NTC under the influence of the metal ion, as shown in Fig. 2. Such a transformation has been observed in $\{[\text{Cd}_2(\text{H}_2\text{Me}_4\text{bpz})(\text{ntcaa})_2(\text{H}_2\text{O})]\cdot \text{H}_2\text{O}\}_n$ ($\text{ntcaa} = 1,4,5,8\text{-NTC}^{2-}$).²⁷ In a marked contrast, in **7**, the metal ion is coordinated with the unmodified 1,4,5,8- NTC^{4-} .

On the other hand, in CPs **4** and **5a**, the starting L^3 has been transformed to L^5 , indicating the hydrolysis of L^3 to form oxalic acid and 3-aminopyridine, as shown in Fig. 3, followed by the reaction of 3-aminopyridine with 1,4,5,8-naphthalenetetracarboxylic dianhydride (1,4,5,8- NTC'') to establish L^5 . Oxalic acid was found co-crystallizing in the crystal structure of **4**. To confirm the formation of L^5 and **5a**, L^5 was synthesized by the reaction of 3-aminopyridine and NTC'' ,²³ which was then reacted with 1,4,5,8- H_4NTC and $\text{Cd}(\text{II})$ salt to afford **5b**.

Structures of $[\text{Cd}(\text{L}^1)_{0.5}(1,4,5,8\text{-NTC})(\text{H}_2\text{O})_2]_n$, **1, $\{[\text{Zn}(\text{L}^2)_{0.5}(1,4,5,8\text{-NTC})(\text{H}_2\text{O})_2]\cdot \text{H}_2\text{O}\}_n$, **2**, and $\{[\text{Cd}(\text{L}^2)_{0.5}(1,4,5,8\text{-NTC})(\text{H}_2\text{O})_2]\cdot \text{H}_2\text{O}\}_n$, **3**.** Single-crystal X-ray diffraction analyses show that CPs **1–3** crystallize in the triclinic space group $P\bar{1}$, with each asymmetric unit consisting of one $\text{M}(\text{II})$ ($\text{M} = \text{Cd}$, **1**; Zn , **2**; Cd , **3**) cation, a half of a bpba ligand ($\text{bpba} = \text{L}^1$, **1**; L^2 , **2** and **3**), one 1,4,5,8- NTC^{2-} ligand and two coordinated water molecules, as well as one co-crystallized water molecule in each of **2** and **3**. Fig. 4(a)–(c) depict drawings showing the coordination environments about the metal ions of **1–3**. Both the $\text{Cd}(\text{II})$ ion of **1** and $\text{Zn}(\text{II})$ ion of **2** adopt the distorted square pyramidal geometry ($\tau_5 = 0.30$, **1**; 0.05, **2**).²⁸ The $\text{Cd}(\text{II})$ ion of **1** is coordinated by two oxygen atoms from two different 1,4,5,8- NTC^{2-} ligands [$\text{Cd–O} = 2.1876(19)–2.1933(18)$ Å], two oxygen atoms from two coordinated water molecules [$\text{Cd–O} = 2.230(3)–2.368(8)$ Å] and one pyridyl nitrogen atoms from the L^1 ligand [$\text{Cd–N} = 2.271(2)$ Å], whereas the $\text{Zn}(\text{II})$ center of **2** is coordinated by two oxygen atoms from two different 1,4,5,8- NTC^{2-} ligands [$\text{Zn–O} = 2.049(3)–2.060(3)$ Å], two oxygen atoms from two coordinated water molecules [$\text{Zn–O} = 2.026(3)–2.114(3)$ Å] and one pyridyl nitrogen atoms from the L^2 ligand [$\text{Cd–N} = 2.069(4)$ Å]. On the other hand, the $\text{Cd}(\text{II})$ ion of **3** is coordinated by three oxygen atoms from two different 1,4,5,8- NTC^{2-} ligands [$\text{Cd–O} = 2.226(4)–2.534(4)$ Å], two oxygen atoms from two coordinated water molecules [$\text{Cd–O} = 2.250(4)–2.336(4)$ Å] and one pyridyl nitrogen atoms from the L^2 ligand [$\text{Cd–N} = 2.253(5)$ Å], resulting in a distorted octahedral geometry.

The metal ions are further linked together by 1,4,5,8- NTC^{2-} and bpba ligands to afford 1D decorated zigzag



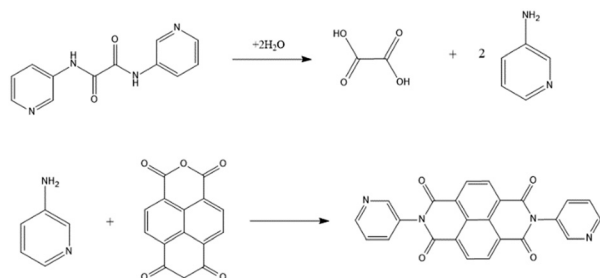


Table 1 Crystallographic data for 1–7

| CP/complex | 1 | 2 | 3 | 4 | 5a | 5b | 6 | 7 |
|---|--|--|--|--|--|--|--|---|
| Formula | C ₂₂ H ₁₇ CdN ₂ O ₁₀ | C ₂₁ H ₁₇ ZnN ₂ O ₁₁ | C ₂₁ H ₁₇ CdN ₂ O ₁₁ | C ₃₉ H ₁₀ ZnN ₄ O ₁₄ | C ₃₈ H ₁₈ CdN ₄ O ₁₂ | C ₃₈ H ₂₂ CdN ₄ O ₁₄ | C ₄₂ H ₃₄ Zn ₂ N ₄ O ₂₂ | C ₂₁ H ₁₉ CdN ₄ O _{7.5} |
| Formula weight | 581.77 | 538.73 | 585.77 | 832.95 | 834.96 | 870.99 | 1077.47 | 559.80 |
| Temperature, K | 296(2) | 296(2) | 296(2) | 296(2) | 296(2) | 293(2) | 296(2) | 299(2) |
| Crystal system | Triclinic | Triclinic | Triclinic | Triclinic | Triclinic | Triclinic | Triclinic | Triclinic |
| Space group | <i>P</i> $\bar{1}$ | <i>P</i> $\bar{1}$ | <i>P</i> $\bar{1}$ | <i>P</i> $\bar{1}$ | <i>P</i> $\bar{1}$ | <i>P</i> $\bar{1}$ | <i>P</i> $\bar{1}$ | <i>P</i> $\bar{1}$ |
| <i>a</i> , Å | 7.5267(6) | 8.103(4) | 8.328(3) | 10.256(3) | 10.4465(6) | 10.24(3) | 6.546(4) | 10.1088(13) |
| <i>b</i> , Å | 11.4086(9) | 10.232(5) | 10.399(3) | 12.694(4) | 12.6964(7) | 12.29(4) | 12.633(7) | 10.4401(13) |
| <i>c</i> , Å | 13.3971(10) | 12.720(6) | 12.543(4) | 13.590(5) | 13.5740(8) | 13.58(5) | 12.865(7) | 11.9209(14) |
| α , ° | 114.8797(16) | 97.593(12) | 95.415(6) | 97.295(9) | 97.2892(13) | 97.39(9) | 97.026(19) | 106.047(3) |
| β , ° | 91.182(2) | 99.913(11) | 97.524(6) | 99.972(10) | 99.3233(13) | 99.45(13) | 95.24(2) | 94.160(3) |
| γ , ° | 94.865(2) | 91.322(13) | 92.705(9) | 105.313(8) | 105.7654(13) | 104.61(11) | 96.96(2) | 112.725(3) |
| <i>V</i> , Å ³ | 1037.85(14) | 1028.7(8) | 1070.1(6) | 1652.6(9) | 1681.83(17) | 1604(10) | 1041.9(10) | 1092.2(2) |
| <i>Z</i> | 2 | 2 | 2 | 2 | 2 | 2 | 1 | 2 |
| <i>D</i> _{calc} , Mg m ^{−3} | 1.862 | 1.739 | 1.818 | 1.674 | 1.649 | 1.803 | 1.717 | 1.702 |
| <i>F</i> (000) | 582 | 550 | 586 | 846 | 836 | 876 | 550 | 562 |
| μ (Mo K α), mm ^{−1} | 1.119 | 1.265 | 1.089 | 0.829 | 0.725 | 0.769 | 1.249 | 1.054 |
| Range (2 θ) for data collection, ° | 3.36 ≤ 2 θ ≤ 56.30 | 3.28 ≤ 2 θ ≤ 52.00 | 3.29 ≤ 2 θ ≤ 51.99 | 3.09 ≤ 2 θ ≤ 50.14 | 3.09 ≤ 2 θ ≤ 52.00 | 3.48 ≤ 2 θ ≤ 51.99 | 3.20 ≤ 2 θ ≤ 52.00 | 4.46 ≤ 2 θ ≤ 52.00 |
| Independent reflections | 5049 [R(int) = 0.0363] | 3990 [R(int) = 0.1255] | 4203 [R(int) = 0.0418] | 5836 [R(int) = 0.1137] | 6620 [R(int) = 0.0649] | 6249 [R(int) = 0.0430] | 4092 [R(int) = 0.0829] | 4276 [R(int) = 0.0847] |
| Data/restraints/parameters | 5049/0/332 | 3990/0/316 | 4203/0/316 | 5836/2/508 | 6620/0/496 | 6249/1/519 | 4092/0/316 | 4276/0/302 |
| Quality-of-fit indicator ^c | 1.034 | 1.064 | 1.123 | 1.048 | 1.005 | 1.015 | 1.027 | 1.012 |
| Final <i>R</i> indices [<i>I</i> > 2 σ (<i>I</i>)] ^{a,b} | <i>R</i> ₁ = 0.0332, <i>wR</i> ₂ = 0.0607 | <i>R</i> ₁ = 0.0742, <i>wR</i> ₂ = 0.0917 | <i>R</i> ₁ = 0.0493, <i>wR</i> ₂ = 0.1295 | <i>R</i> ₁ = 0.0838, <i>wR</i> ₂ = 0.2025 | <i>R</i> ₁ = 0.0438, <i>wR</i> ₂ = 0.0852 | <i>R</i> ₁ = 0.0467, <i>wR</i> ₂ = 0.1104 | <i>R</i> ₁ = 0.0463, <i>wR</i> ₂ = 0.0899 | <i>R</i> ₁ = 0.0378, <i>wR</i> ₂ = 0.0598 |
| <i>R</i> indices (all data) | <i>R</i> ₁ = 0.0517, <i>wR</i> ₂ = 0.0663 | <i>R</i> ₁ = 0.1386, <i>wR</i> ₂ = 0.1055 | <i>R</i> ₁ = 0.0565, <i>wR</i> ₂ = 0.1334 | <i>R</i> ₁ = 0.1468, <i>wR</i> ₂ = 0.2372 | <i>R</i> ₁ = 0.0675, <i>wR</i> ₂ = 0.0926 | <i>R</i> ₁ = 0.0716, <i>wR</i> ₂ = 0.1226 | <i>R</i> ₁ = 0.0857, <i>wR</i> ₂ = 0.1029 | <i>R</i> ₁ = 0.0636, <i>wR</i> ₂ = 0.0655 |

^a $R_1 = \sum ||F_o| - |F_c|| / \sum |F_o|$. ^b $wR_2 = [\sum w(F_o^2 - F_c^2)^2 / \sum w(F_o^2)]^{1/2}$. ^c $w = 1/[\sigma^2(F_o^2) + (ap)^2 + (bp)]$, $p = [\max(F_o^2 \text{ or } 0) + 2(F_c^2)]/3$. $a = 0.0482$, $b = 0.4052$ for 1; $a = 0.0229$, $b = 0.5143$ for 2; $a = 0.0749$, $b = 2.0348$ for 3; $a = 0.1042$, $b = 8.3159$ for 4; $a = 0.0596$, $b = 2.4584$ for 5a; $a = 0.0666$, $b = 0.0000$ for 5b; $a = 0.0426$, $b = 0.1291$ for 6; $a = 0.0210$, $b = 0.0000$ for 7. ^c Quality-of-fit = $[\sum w(|F_o|^2 - |F_c|^2)^2 / (N_{\text{observed}} - N_{\text{parameters}})]^{1/2}$.

Fig. 3 Formation pathways for L^5 .



Structures of $\{[\text{Zn}(\text{L}^5)(1,4,5,8\text{-NTC})(\text{H}_2\text{O})]\cdot 0.5\text{OA}\}_m$, **4, $[\text{Cd}(\text{L}^5)(1,4,5,8\text{-NTC})(\text{H}_2\text{O})]_m$, **5a**, and $\{[\text{Cd}(\text{L}^5)(1,4,5,8\text{-NTC})(\text{H}_2\text{O})]\cdot 2\text{H}_2\text{O}\}_m$, **5b**.** The crystal structures of CPs **4**, **5a** and **5b** were in the triclinic space group $P\bar{1}$. Each of the asymmetric units consists of one $\text{M}(\text{II})$ cation ($\text{M} = \text{Zn}$, **4**; Cd , **5a**; Cd , **5b**), two halves of an L^5 ligand, one 1,4,5,8- NTC^{2-} ligand and one coordinated water molecule. In addition, there are a half of a co-crystallized oxalic acid in **4** and two cocrystallized water molecule in **5b**, respectively. Fig. 6(a) depicts a representative drawing showing the coordination environment about the metal ion, which is five-coordinated by two oxygen atoms from two 1,4,5,8- NTC^{2-} ligands [$\text{Zn}-\text{O} = 2.063(5)\text{--}2.084(6)$ Å for **4**; $\text{Cd}-\text{O} = 2.234(3)\text{--}2.246(3)$ Å for **5a**; $\text{Cd}-\text{O} = 2.234(3)\text{--}2.246(3)$ Å for **5b**], one oxygen atom from the coordinated water molecule [$\text{Zn}-\text{O} = 2.029$ (5) Å for **4**; $\text{Cd}-\text{O} = 2.231(2)$ Å for **5a**; $\text{Cd}-\text{O} = 2.231(2)$ Å for **5b**] and two pyridyl nitrogen atoms from two different L^5 ligands [$\text{Cd}-\text{N} = 2.084(6)\text{--}2.119(6)$ Å for **4**; $\text{Cd}-\text{N} = 2.292(3)\text{--}2.279(3)$ Å for **5a**; $\text{Cd}-\text{N} = 2.292(3)\text{--}2.279(3)$ Å for **5b**], resulting in a distorted square pyramidal geometry ($\tau_5 = 0.03$ for **4**; 0.06 for **5a**; 0.03 for **5b**). The $\text{M}(\text{II})$ ions are further linked by 1,4,5,8- NTC^{2-} and L^5 ligands to afford a 2D structure. If the $\text{M}(\text{II})$ ions are defined as 4-connected nodes and 1,4,5,8- NTC^{2-} ligands as 2-connected nodes, while L^5 as linkers, the structures of these CPs can be regarded as 2D nets with the $\{4\cdot 8^5\}\{4\text{--}2,4\text{L1}\}$ topology,

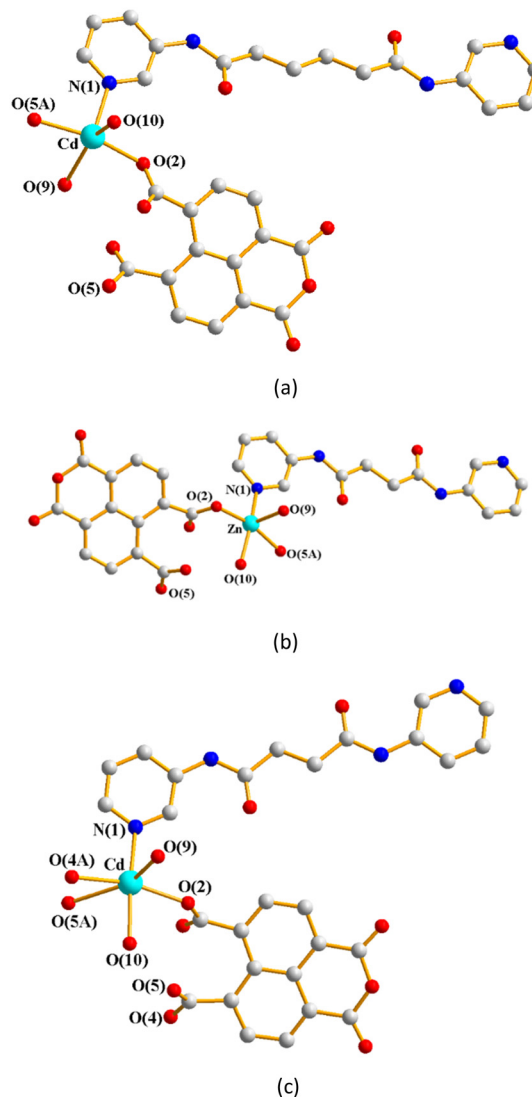


Fig. 4 (a) Coordination environment about the Cd(II) ion of **1**. Symmetry transformations used to generate equivalent atoms: (A) $-x, -y + 2, -z + 2$. (b) Coordination environment about the Zn(II) ion of **2**. Symmetry transformations used to generate equivalent atoms: (A) $-x - 1, -y + 2, -z + 1$. (c) Coordination environment about the Cd(II) ion of **3**. Symmetry transformations used to generate equivalent atoms: (A) $-x + 1, -y + 1, -z$.

Fig. 6(b). Similar to 1–3, the structural types of 4–5 are subject to the formation of 1,4,5,8-NTC'²⁻.

Structure of $[\text{Zn}_2(\text{L}^4)(1,4,5,8\text{-NTC})_2(\text{H}_2\text{O})_6]$, **6.** Crystals of complex **6** conform to the triclinic space group $P\bar{1}$ and the asymmetric unit comprises one $\text{Zn}(\text{II})$ cation, a half of an L^4 ligand, one 1,4,5,8-NTC²⁻ ligand and three coordinated water molecules. Fig. 7(a) depicts a drawing showing the dinuclear structure of **6**, in which the two $\text{Zn}(\text{II})$ ions are bridged by the L^4 ligand. Each of the two $\text{Zn}(\text{II})$ ions is six-coordinated by two oxygen atoms from the 1,4,5,8-NTC²⁻ ligand [$\text{Zn}-\text{O} = 2.203(3)\text{--}2.230(3)$ Å], three oxygen atoms from three coordinated water molecules [$\text{Zn}-\text{O} = 2.039(3)\text{--}2.154(3)$ Å] and one pyridyl nitrogen atoms from the L^4 ligand [$\text{Zn}-\text{N} = 2.061(3)$ Å], resulting in a distorted octahedral geometry.

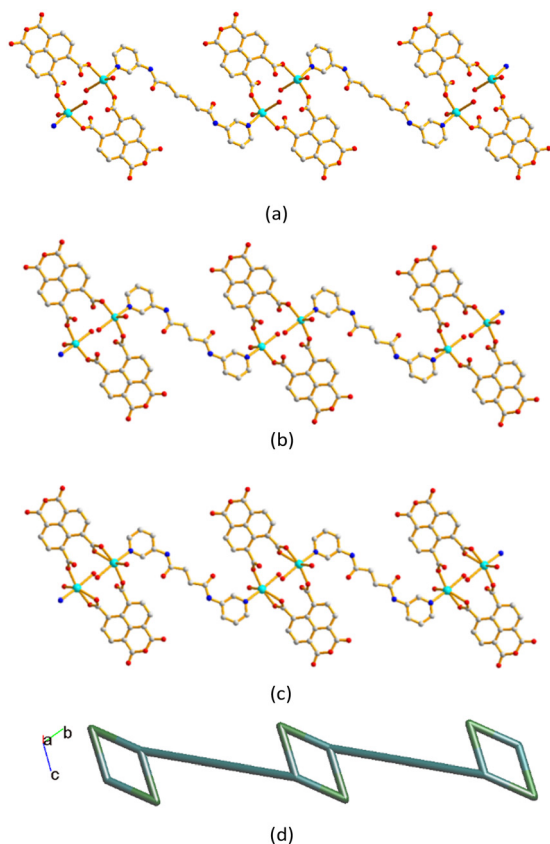


Fig. 5 Drawings showing the 1D decorated zigzag chains of (a) **1**, (b) **2** and (c) **3**. (d) A representative topological structure showing a 1D looped chain with the (4)-2,3C2 topology.

Moreover, the dinuclear molecules are interlinked extensively through O—H—O [O—H...O = 2.1010–2.2237 Å] hydrogen bonds. Considering molecules of **6** as nodes that are linked by the hydrogen bonds, a topological $(4^{12} \cdot 6^3)$ -pcu supramolecular structure can be obtained, as shown in Fig. 7(b).

Structure of $[\{\text{Cd}(\text{L}^4)(1,4,5,8\text{-NTC})_{0.5}(\text{H}_2\text{O})\} \cdot 0.5\text{H}_2\text{O}]_m$, **7.** CP **7** crystallizes in the triclinic space group $P\bar{1}$ and the asymmetric unit consists of one Cd(II) cation, two halves of an L^4 ligand, a half of a $1,4,5,8\text{-NTC}^{4-}$ ligand, one coordinated water molecule, and a half of a cocrystallized water molecule. Fig. 8(a) depicts a drawing showing the coordination environment about of Cd(II) ion of **7**, which is five-coordinated by two oxygen atoms from two $1,4,5,8\text{-NTC}^{4-}$ ligands [Cd—O = 2.227(2)–2.229(2) Å], one oxygen atom from the coordinated water molecule [Cd—O = 2.279(2) Å] and two pyridyl nitrogen atoms from two L^4 ligands [Cd—N = 2.271(2) Å], resulting in a distorted square pyramidal geometry ($\tau_5 = 0.21$). The Cd(II) ions are further linked together by $1,4,5,8\text{-NTC}^{4-}$ and L^4 ligands to afford a 3D structure. If the Cd(II) atoms are defined as 4-connected nodes, $1,4,5,8\text{-NTC}^{4-}$ as 4-connected nodes, while L^4 as linkers, the structure of CP **7** can be simplified as a 3D net with the $\{4 \cdot 6^4 \cdot 8\}_2\{4^2 \cdot 6^2 \cdot 8^2\}$ -mog topology, Fig. 8(b). A structural comparison of **6** and **7**

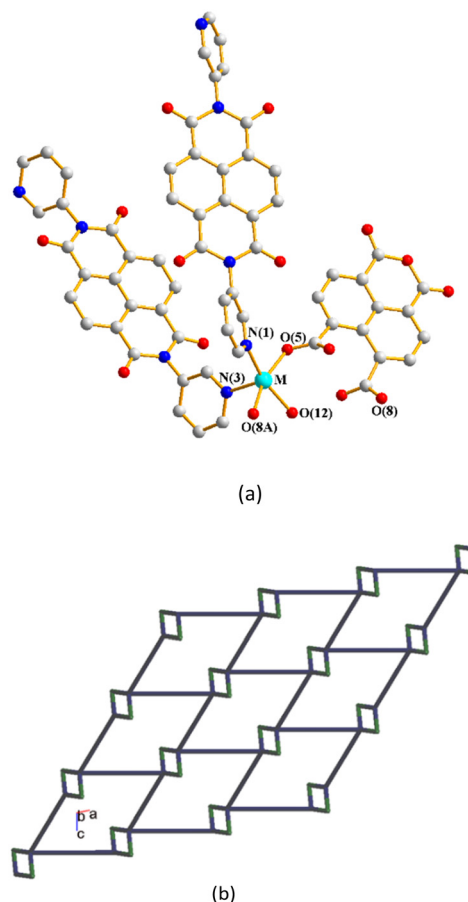


Fig. 6 (a) A representative drawing for the coordination environment about the metal ion of **4** (M = Zn), **5a** (M = Cd) and **5b** (M = Cd). Symmetry transformations used to generate equivalent atoms: (A) $-x + 2, -y + 2, -z + 1$ for **4**, (A) $-x + 1, -y, -z - 2$ for **5a** and (A) $-x, -y + 1, -z + 2$ for **5b**. (b) A representative topological structure showing a 2D net with the 2,4L1 topology.

indicates that the metal identity governs the structural diversity.

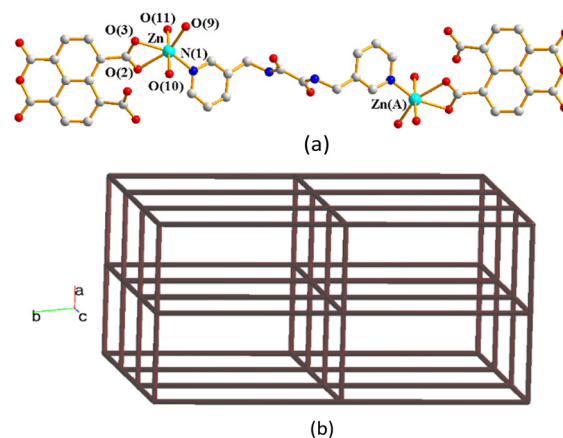


Fig. 7 (a) A drawing showing the dinuclear structure of **6**. Symmetry transformations used to generate equivalent atoms: (A) $-x + 1, -y + 1, -z + 2$. (b) A drawing showing the supramolecular structure of **6** with the pcu topology.



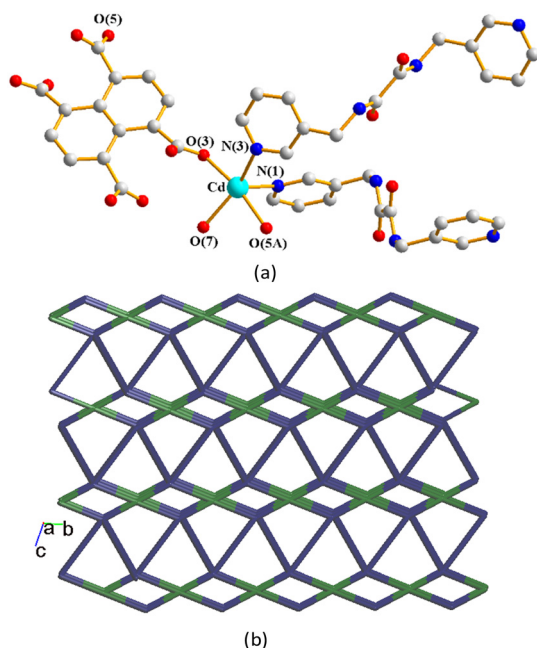


Fig. 8 Coordination environment about the Cd(II) ion of **7**. Symmetry transformations used to generate equivalent atoms: (A) $x - 1, y - 1, z$. (b) A drawing showing the 3D net with the **mog** topology.

Ligand conformations and bonding modes

The **L**¹ and **L**² can be arranged in A and G conformations when the C–C–C–C torsion angle (θ) is $180^\circ \geq \theta > 90^\circ$ and $0^\circ \leq \theta \leq 90^\circ$, respectively, and based on the relative orientation of the C=O groups, each conformation can adopt a *cis* or *trans* arrangement.¹² Due to the difference in the orientations of the pyridyl nitrogen atom positions, three more orientations, *anti-anti*, *syn-anti* and *syn-syn*, are possible for the ligands **L**¹, **L**² and **L**⁴. By determining the orientation of the nitrogen on the pyridine, the conformation of **L**⁵ can be classified into *cis* or *trans*. Accordingly, the ligand conformations of **1–7** are assigned and listed in Table 2. On the other hand, the polycarboxylate ligands show various coordination modes in **1–7**. While the 1,4,5,8-NTC²⁻ ligands in **1**, **2**, **4**, **5a**, and **5b** bridge two metal ions through two of the carboxylate oxygen atoms, that in **3** bridges two metal ions through a chelation mode. In complex **6**, the 1,4,5,8-NTC²⁻ ligand chelates a metal ion through the two oxygen atoms of one carboxylate group, and the 1,4,5,8-NTC⁴⁻ ligand in **7** bridges four metal ions through four oxygen atoms from four carboxylate groups.

Powder X-ray analysis

In order to check the bulk purities of the products, powder X-ray diffraction (PXRD) patterns have been measured for **1–7**. As shown in Fig. S1–S8,† the peak positions of the experimental and simulated PXRD patterns are in agreement with each other, which demonstrate that the crystal structures are representative of the bulk materials. The

differences in intensity may be owing to the preferred orientation of the powder samples.

Thermal properties

Thermal gravimetric analysis (TGA) was carried out to examine the thermal decomposition of **1–7**. The samples were recorded from about 30 to 800 °C at 10 °C min^{−1} under a N₂ atmosphere, as shown in Fig. S9–S16† and Table 3. Two-step decompositions involving losses of solvents and organic ligands are observed.

Chemical stability

To select the solvent for subsequent metal ion sensing experiments, 10 mg of each of **1–3**, **6**, and **7** was immersed in 10 ml of 10 different solvents for seven days. Afterward, the samples were vacuum-dried and PXRD patterns measured. As shown in Fig. S17–S21,† **1** and **7** maintain their crystal structures in all of the 10 different solvents, whereas **2** undergoes complete structural changes in DMF and dissolves completely in DMA, whereas **3** experiences complete collapse of its crystal structure in MeOH, DMA and DMF and **6** shows structural changes in DMA, DMF and ether. The results indicate that these **1–7** are stable in water for seven days.

Luminescent properties

The excitation and emission spectra of **L**¹, **L**², and **L**⁴ and **1–3**, **6**, and **7** in the solid state are shown in Fig. S22–S26.† Table 4 lists their corresponding parameters. The spectra of **L**¹, **L**², **L**⁴ and 1,4,5,8-H₄NTC show emissions in the range of 459–496 nm, which may be ascribed to the intraligand (IL) n to π^* or π to π^* transitions. Since Zn(II) and Cd(II) ions are not easily oxidized or reduced, the emissions of **1–3**, **6**, and **7**, which are in the range 404–510 nm, are not due to ligand-to-metal charge transfer (LMCT) or metal-to-ligand charge transfer (MLCT), but most probably ligand-to-ligand charge transfer (LLCT) or intra-ligand charge transfer.^{30,31}

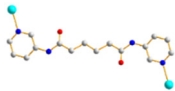
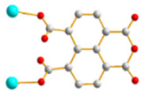
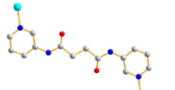
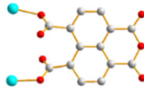
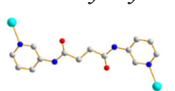
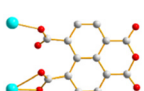
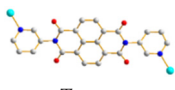
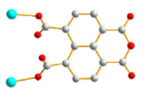
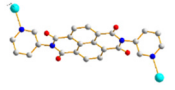
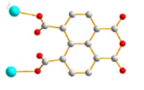
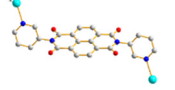
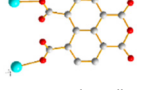
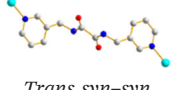
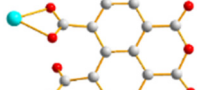
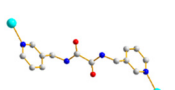
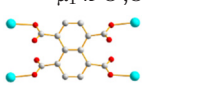
Metal cation detection

For each experiment, 30 mg of the sample was immersed in 10 mL of 10^{−2} M aqueous solutions of different metal ions, involving Fe(NO₃)₃ and M(OAc)₂ (M = Fe²⁺, Co²⁺, Ni²⁺, Cu²⁺, Zn²⁺) at room temperature for 24 hours. The sample was filtered, washed with water and dried under vacuum, and then its solid-state emission spectrum measured. Fig. S27–S31† display the emission spectra and the bar charts showing the percentages of quenching of **1–3**, **6**, and **7**. Fig. 9 depicts the bar charts showing the average quenching percentages of three experiments. The percentages of quenching of **1–3**, **6**, and **7** toward Fe³⁺ are 66, 71, 64, 80 and 90%, respectively, indicating that **7** affords the best quenching efficiency.

Electron transfer, structure collapse, competitive absorption, and cation exchange are the main causes of fluorescence quenching.³² The PXRD patterns of **7** before and after immersion in Fe³⁺ solution are thus compared. Fig.



Table 2 Ligand conformations and bonding modes of 1–7

| CP/complex | Ligand conformation | Coordination mode |
|------------|---|---|
| 1 |  AAA <i>trans syn-syn</i> |  $\mu_2\text{-}\kappa\text{O}':\kappa\text{O}''$ |
| 2 |  A <i>trans syn-syn</i> |  $\mu_2\text{-}\kappa\text{O}':\kappa\text{O}''$ |
| 3 |  A <i>trans syn-syn</i> |  $\mu_2\text{-}\kappa^2\text{O}',\text{O}'':\kappa\text{O}'''$ |
| 4 |  <i>Trans</i> |  $\mu_2\text{-}\kappa\text{O}':\kappa\text{O}''$ |
| 5a |  <i>Trans</i> |  $\mu_2\text{-}\kappa\text{O}':\kappa\text{O}''$ |
| 5b |  <i>Trans</i> |  $\mu_2\text{-}\kappa\text{O}':\kappa\text{O}''$ |
| 6 |  <i>Trans syn-syn</i> |  $\mu_1\text{-}\kappa^2\text{O}',\text{O}''$ |
| 7 |  <i>Trans syn-syn</i> |  $\mu_4\text{-}\kappa\text{O}':\kappa\text{O}'':\kappa\text{O}''':\kappa\text{O}''''$ |

S32[†] indicates that no significant change of the PXRD patterns can be observed, revealing that the quenching is not due to the structural collapse. Fig. S33[†] shows that the absorption spectrum of the Fe³⁺ solution partially overlaps with the excitation spectrum of 7, therefore, the fluorescence quenching can be ascribed to competitive absorption. SEM-EDX spectra, as shown in Fig. S34[†] demonstrate that Fe³⁺ ions are indeed adsorbed by 7.

FT-IR and XPS spectroscopy are applied for the investigation of the interactions between the Fe³⁺ ion and 7. As shown in Fig. S35[†] the amide C=O stretching frequency shifted slightly from $\nu = 1676\text{ cm}^{-1}$ to $\nu = 1659\text{ cm}^{-1}$, indicating a red shift due to the weak interaction between Fe³⁺ and the amide oxygen atom. Fig. S36[†] shows the XPS spectra of 7 before and after immersing in Fe³⁺. The fitting analysis reveals four signals at 531.0, 531.8, 532.5 and 533.8 eV, Fig. S37[†] assignable to O*=C–N, O*=C–O, O=C–O* and H₂O*, respectively.^{33,34} There is no significant change in the

binding energy of O 1s electrons before and after the sensing experiments, therefore, the changes in the intensities are evaluated. The intensity of the peak at 531.0 eV decreased from 19 to 11%, while that at 531.8 eV increased from 39 to 45%, indicating the possible interaction between the oxygen atom of O*=C–N and Fe³⁺, which further verifies the result from the investigation of the IR spectra.

Quenching efficiency

To understand the dependence of the quenching efficiency of 7 on the concentration of Fe³⁺ ions in aqueous solution, the sample of 7 was immersed in solutions of different concentrations (0.25–6 mM) of Fe³⁺ for 24 hours, followed by the measurement of the emission spectrum after immersion. The quenching efficiency of Fe³⁺ ions by 7 was analyzed by using the Stern-Volmer (SV) equation: $(I_0/I) = 1 + K_{SV}[M]$,³⁵ where I_0 is the emission intensity of the intact



Table 3 Weight loss of 1–7

| CP/complex | Solvent, T, °C (found/calc), % | Ligand, T, °C (found/calc), % |
|------------|--|--|
| 1 | 2H ₂ O 30–190 (6.19/5.62) | L ¹ + 1,4,5,8-NTC' ²⁻ 230–800 (74.49/79.39) |
| 2 | 3H ₂ O 30–190 (3.18/4.25) | L ² + 1,4,5,8-NTC' ²⁻ 235–800 (74.60/79.15) |
| 3 | 2.5H ₂ O 30–153 (9.04/9.22) | L ² + 1,4,5,8-NTC' ²⁻ 240–800 (72.41/71.58) |
| 4 | 1H ₂ O + 0.5EDA 30–143 (9.33/7.57) | L ⁵ + 1,4,5,8-NTC' ²⁻ 320–800 (76.16/84.13) |
| 5a | 1H ₂ O 30–88 (4.67/2.11) | L ⁵ + 1,4,5,8-NTC' ²⁻ 192–800 (79.48/82.61) |
| 5b | 2H ₂ O 30–100 (7.06/4.14) | L ⁵ + 1,4,5,8-NTC' ²⁻ 147–800 (78.90/82.63) |
| 6 | 2H ₂ O 30–100 (10.30/10.03) | L ⁴ + 1,4,5,8-NTC' ²⁻ 180–800 (77.64/77.83) |
| 7 | 1.75H ₂ O 30–173 (3.33/4.05) | L ⁴ + 1,4,5,8-NTC' ⁴⁻ 200–900 (75.61/75.84) |

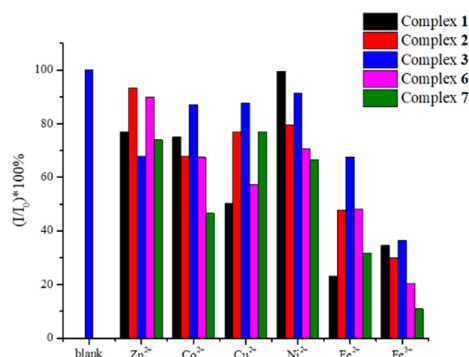


Fig. 9 Bar charts showing the average quenching percentages of the 1–3, 6, and 7 in the various cations.

sample, I is the emission intensity after immersion, K_{SV} is the quenching constant and $[M]$ is the molar concentration of Fe^{3+} ion. Fig. S38† shows the dependence of emission intensity of 7 on the concentration of Fe^{3+} ions, which decreases as the concentration of Fe^{3+} ions increases. Fig. 10 displays the Stern–Volmer (SV) plot of Fe^{3+} ions, indicating that at low concentrations (6–0.25 mM), the variation of (I_0/I) is linear, giving $1.06 \times 10^3 M^{-1}$ and $1.99 \times 10^{-4} M$ for the Stern–Volmer constant (K_{SV}) and the limit of detection (LOD), respectively.

Recycling capability

To evaluate the recycling capability, CP 7 was immersed in Fe^{3+} solution for one day, filtered, washed with water and then subjected to the measurement of PXRD patterns. As shown in Fig. S39† the structure of 7 may probably remain stable for five cycles.

Gas adsorption

N_2 adsorption measurements of 1, 2, 3, 6, and 7 were conducted at 77 K, with the results shown in Fig. S40–

Table 4 The excitation and emission wavelengths of 1–3, 6, and 7 in solid state

| Compound | λ_{ex} (nm) | λ_{em} (nm) | Compound | λ_{ex} (nm) | λ_{em} (nm) |
|----------------|---------------------|---------------------|----------------------------|---------------------|---------------------|
| L ¹ | 411 | 459 | L ⁴ | 347 | 473 |
| L ² | 368 | 496 | 1,4,5,8-H ₄ NTC | 400 | 472 |
| 1 | 338 | 404 | 6 | 405 | 445 |
| 2 | 367 | 510 | 7 | 442 | 500 |
| 3 | 410 | 443 | | | |

S49.† The BET surface areas of 1, 2, 3, 6 and 7 are 273.32, 180.59, 266.25, 418.44 and 102.61 $m^2 g^{-1}$, respectively. Additionally, the pore-size distribution curves show that the pore sizes of 1, 2, 3, 6 and 7 are 6.22, 7.77, 8.26, 7.02 and 5.99 nm, respectively. While 7 gives the best quenching efficiency, its BET surface area and pore size are not the largest among 1, 2, 3, 6 and 7, indicating the stable 3D framework of 7 may enhance the quenching efficiency.

Conclusions

Seven new CPs and one dinuclear complex ranging from 0D to 1D, 2D and 3D CPs have been successfully synthesized through hydrothermal reactions by using bpba, 1,4,5,8-H₄NTC and metal salt. Ligand transformations from 1,4,5,8-H₄NTC to 1,4,5,8-H₂NTC'²⁻ and L³ to L⁵ are observed in 1–6, whereas in 7, the 1,4,5,8-NTC'⁴⁻ anion retains its structure. CPs 1, 2, and 3 exhibit 1D chains with the 2,3C2 topology and 4, 5a, and 5b show 2D layers with the 2,4L2 topology, whereas 6 is dinuclear, exhibiting a 3D supramolecular structure with the **pcu** topology, and 7 has a 3D structure with the **mog** topology. The structural diversities of 1–7 are subject to the formation of 1,4,5,8-NTC' and the identities of the bpba ligands. CPs 1, 2, 3 and 7 and the dinuclear complex 6 exhibit fluorescence properties, giving the 3D 7 the highest potential for detecting Fe^{3+} ions in aqueous solution with $1.06 \times 10^3 M^{-1}$ and $1.99 \times 10^{-4} M$ for K_{SV} and LOD, respectively.

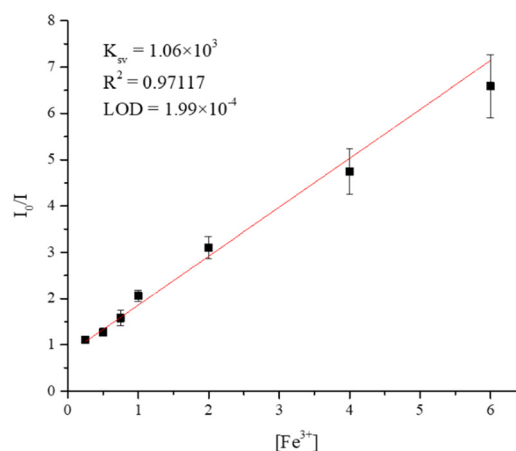


Fig. 10 The SV plot of 7.



Data availability

The data supporting this article have been included as part of the ESI.† Crystallographic data for complexes 1–7 has been deposited at the CCDC with no. 2395512–2395519.

Author contributions

Investigation, W.-H. C.; data curation, Y.-H. C.; review and supervision, K. B. T., S.-M. L. and J.-D. C. All authors have read and agreed to the published version of the manuscript.

Conflicts of interest

There are no conflicts to declare.

Acknowledgements

We are grateful to National Science and Technology Council of the Republic of China for support.

References

- 1 S. R. Batten, N. R. Champness, X.-M. Chen, J. Garcia-Martinez, S. Kitagawa, L. Öhrström, M. O'Keeffe, M. P. Suh and J. Reedijk, *Pure Appl. Chem.*, 2013, **85**, 1715–1724.
- 2 E. R. T. Tiekink and J. J. Vittal, *Frontiers in Crystal Engineering*, John Wiley & Sons, Ltd., England, 2006.
- 3 C.-Yi. Lee, M. Usman, S.-W. Wang, K. B. Thapa, T.-R. Chen and J.-D. Chen, *CrystEngComm*, 2024, **26**, 5099–5107.
- 4 C.-Yi. Lee, Y.-H. Ye, S.-W. Wang and J.-D. Chen, *Molecules*, 2024, **29**, 1748.
- 5 X.-K. Yang, W.-T. Lee, J.-H. Hu and J.-D. Chen, *CrystEngComm*, 2021, **23**, 4486–4493.
- 6 C.-J. Chen, C.-L. Chen, T.-H. Liu, W.-T. Lee, J.-H. Hu, P. M. Chhetri and J.-D. Chen, *Chemistry*, 2021, **3**, 1–12.
- 7 K. B. Thapa and J.-D. Chen, *CrystEngComm*, 2015, **17**, 4611–4626.
- 8 T.-T. Liao, M. Usman, Y.-H. Ye, K. B. Thapa and J.-D. Chen, *Inorg. Chim. Acta*, 2023, **574**, 122368.
- 9 X. Yan, J. Lei, Y.-P. Li, P. Zhang and Y. Wang, *CrystEngComm*, 2022, **24**, 2264–2269.
- 10 S. R. Batten, S. M. Neville and D. R. Turner, *Coordination Polymers: Design, Analysis and Application*, Royal Society of Chemistry, Cambridge, UK, 2009.
- 11 S. Li, B. Wang, G. Liu, X. Li, C. Sun, Z. Zhang and X. Wang, *Inorg. Chem. Front.*, 2024, **11**, 1561–1572.
- 12 M. Govindaraj, S.-Y. Zhong, C.-H. Lin and J.-D. Chen, *Molecules*, 2023, **28**, 2226.
- 13 F. Nie and D. Yan, *Angew. Chem., Int. Ed.*, 2023, **62**, e202302751.
- 14 X.-Y. Ren, F.-Y. Chen, C.-H. Zhang, Z.-G. Liang, X.-Y. Yu, S.-D. Han and G.-M. Wang, *Chem. – Eur. J.*, 2024, **30**, e202402581.
- 15 X.-G. Yang, Y.-J. Chen, P.-P. Yin, Y. Li, S.-Y. Yang, Y.-M. Li and L.-F. Ma, *Chem. Sci.*, 2024, **15**, 14202–14208.
- 16 X.-G. Yang, J.-H. Qin, Y.-D. Huang, Z.-M. Zhai, L.-F. Ma and D. Yan, *J. Mater. Chem. C*, 2020, **8**, 17169–17175.
- 17 Y. Chen, A.-G. Liu, P.-D. Liu, Z.-T. Chen, S.-Y. Liu and B. Li, *J. Mater. Chem. A*, 2023, **11**, 18236–18246.
- 18 G. C. Liu, Y. Li, J. Chi, N. Xu, X. L. Wang, H. Y. Lin and Y. Q. Chen, *Dyes Pigm.*, 2020, **174**, 108064.
- 19 B. Fu, J. Chen, Y. Cao, H. Li, F. Gao, D.-Y. Guo, F. Wang and Q. Pan, *Sens. Actuators, B*, 2022, **369**, 132261.
- 20 Y.-F. Liu, J.-H. Hu, W.-T. Lee, X.-K. Yang and J.-D. Chen, *Cryst. Growth Des.*, 2020, **20**, 7211–7218.
- 21 T.-T. Liao, S.-Y. Lin and J.-D. Chen, *CrystEngComm*, 2023, **25**, 1723–1730.
- 22 Y.-H. Liu, T.-T. Liao, S.-Y. Lin, S.-Y. Zhong, T.-R. Chen and J.-D. Chen, *Inorg. Chim. Acta*, 2023, **556**, 121641.
- 23 S. Fang, E. Li, D. Zhu, G. Wu, Q. Zhang, C. Lin, F. Huang and H. Li, *Chem. Commun.*, 2021, **57**, 6074–6077.
- 24 Bruker AXS, APEX2, V2008.6; SAD ABS V2008/1; SAINT +V7.60A; SHELXTL V6.14, Bruker AXS Inc., Madison, Wisconsin, USA, 2008.
- 25 G. M. Sheldrick, *Acta Crystallogr., Sect. C: Struct. Chem.*, 2015, **71**, 3–8.
- 26 A. L. Spek, *Acta Crystallogr., Sect. C: Struct. Chem.*, 2015, **71**, 9–18.
- 27 Y.-Q. Sun, S. Deng, S.-Z. Ge, Q. Liu and Y.-P. Chen, *J. Cluster Sci.*, 2013, **24**, 605–617.
- 28 A. W. Addison, T. N. Rao, J. Reedijk, J. van Rijn and G. C. Verschoor, *J. Chem. Soc., Dalton Trans.*, 1984, 1349–1356.
- 29 V. A. Blatov, A. P. Shevchenko and D. M. Proserpio, *Cryst. Growth Des.*, 2014, **14**, 3576–3586.
- 30 D. Sun, Z.-H. Yan, V. A. Blatov, L. Wang and D.-F. Sun, *Cryst. Growth Des.*, 2013, **13**, 1277–1289.
- 31 J.-X. Yang, Z. Xin, Y.-Y. Qin and Y.-G. Yao, *Cryst. Growth Des.*, 2020, **20**, 6366–6381.
- 32 M. Pamei and A. Puzari, *Nano-Struct. Nano-Objects*, 2019, **19**, 100364.
- 33 NIST X-ray Photoelectron Spectroscopy Database, *NIST Standard Reference Database Number 20*, National Institute of Standards and Technology, Gaithersburg, M. D., 2000.
- 34 G. Beamson and D. Briggs, *High Resolution XPS of Organic Polymers: The Scienta ESCA300 Database*, Wiley, New York, NY, 1992.
- 35 S. S. Nagarkar, B. Joarder, A. K. Chaudhari, S. Mukherjee and S. K. Ghosh, *Angew. Chem., Int. Ed.*, 2013, **52**, 2881–2885.

